

The pulsation modes, masses and evolution of luminous red giants

P. R. Wood*

Research School of Astronomy and Astrophysics, Australian National University, Cotter Road, Weston Creek ACT 2611, Australia

ABSTRACT

The period–luminosity sequences and the multiple periods of luminous red giant stars are examined using the OGLE III catalogue of long-period variables in the Large Magellanic Cloud. It is shown that the period ratios in individual multimode stars are systematically different from the ratios of the periods at a given luminosity of different period–luminosity sequences. This leads to the conclusion that the masses of stars at the same luminosity on the different period–luminosity sequences are different. An evolutionary scenario is used to show that the masses of stars on adjacent sequences differ by ~ 16 – 26% at a given luminosity, with the shorter period sequence being more massive. The mass is also shown to vary across each sequence by a similar percentage, with the mass increasing to shorter periods. On one sequence, sequence B, the mass distribution is shown to be bimodal. It is shown that the small amplitude variables on sequences A', A and B pulsate in radial and nonradial modes of angular degree $\ell=0, 1$ and 2 , with the $\ell=1$ mode being the most common. The stars on sequences C' and C are predominantly radial pulsators ($\ell=0$). Matching period ratios to pulsation models shows that the radial pulsation modes associated with sequences A', A, B, C' and C are the 4th, 3rd, 2nd and 1st overtones and the fundamental mode, respectively.

Key words: stars: AGB and post-AGB – stars: oscillations – stars: variables: general.

1 INTRODUCTION

It is now well known that luminous red giants are variable and that the periods of the observed variability lie on discrete sequences in period–luminosity diagrams. Wood et al. (1999) and Wood (2000) used data from MACHO observations of stars in the Large Magellanic Cloud (LMC) to define five sequences A, B, C, D and E in the $(I_W, \log P)$ and $(K, \log P)$ planes, respectively (where I_W is a reddening-free Weisenheit index defined as $I - 1.38(V - I)$). The sequences A, B and C were identified as containing pulsating stars, while sequence E was found to consist of binary stars and sequence D was the sequence formed by the long secondary periods (LSPs) that occur in 30–50% of luminous pulsating red giants. In this paper, the pulsating stars will be discussed. These stars lie on sequences A, B and C and two other sequences A' and C' which are described below. Further examination of the ellipsoidal variables on sequence E can be found in Soszyński et al. (2004b), Nicholls, Wood, & Cioni (2010), Nicholls & Wood (2012) and Nie & Wood (2014) while studies of the origins of the LSPs can be found in Hinkle et al. (2002), Olivier & Wood (2003), Wood, Olivier, &

Kawaler (2004), Nicholls et al. (2009), Stothers (2010) and Takayama, Wood, & Ita (2015).

Following the discovery of sequences A, B and C, Ita et al. (2004) used extensive K band photometry combined with MACHO periods to show that sequence B was in fact two sequences which were renamed B and C'. The next refinement to the luminous sequences was by Soszyński et al. (2004a) who used OGLE data to show the existence of a new sequence on the short period side of sequence A. Soszyński et al. (2004a) labelled this sequence a_4 but in this paper the designation A' will be used (e.g. Derekas et al. 2006; Tabur et al. 2010; Soszyński, Wood, & Udalski 2013). Soszyński et al. (2004a) also made the important discovery that sequence A consisted of three closely-spaced parallel sequences. Soszyński et al. (2007) claimed that sequences B and A' also consisted of three closely-spaced parallel sequences (hereinafter referred to as sub-sequences). More recently, Soszyński & Wood (2013) have drawn attention to a probable faint sequence designated F between sequences C' and C.

Wood et al. (1999) assumed that all the variable luminous red giants found by the MACHO observations were asymptotic giant branch (AGB) stars. However, Ita et al. (2002) and Kiss & Bedding (2003) showed that both AGB and red giant branch (RGB) stars were variable and that

* E-mail: peter.wood@anu.edu.au

there was a slight offset in period between the sequences of RGB and AGB stars. Soszyński et al. (2004a) also noted this offset but they did not find evidence for two slightly offset sequences for sequence A' which they suggested consisted of AGB stars only. However, this result was challenged by Tabur et al. (2010) who showed that an RGB component of sequence A' does exist.

Various attempts have been made to identify the pulsation modes associated with the pulsation sequences C, C', B, A and A' and the sub-sequences of B, A and A'. Wood et al. (1999) (see also Wood & Sebo 1996) showed that the radial fundamental mode could fit sequence C with reasonable assumptions about the mass of the star and that the first few radial overtone modes had periods similar to those of sequences B (which now includes C') and A, although the data available at the time was not extensive enough for a detailed matching of these latter sequences with modes. They also noted that the large-amplitude Mira variables fell on sequence C, making them fundamental mode pulsators. Additional evidence in favour of this modal assignment is provided by the fact that nonlinear fundamental mode radial pulsation models reproduce the light and velocity curves of local Mira variables quite well (e.g. Bessell, Scholz, & Wood 1996; Ireland, Scholz, & Wood 2008). Recently, using extensive observational data from OGLE, Soszyński & Wood (2013) showed that the period ratios in stars of sequences C and C' were consistent with those expected for fundamental mode pulsation of sequence C and first overtone pulsation on sequence C'. Takayama, Saio, & Ita (2013) compared period ratios for OGLE variables near the tip of the RGB with models and concluded that sequences C', B and A corresponded to the radial first, second and third overtones, consistent with the assignments by Wood et al. (1999) and Soszyński & Wood (2013).

In contrast to the above results, Soszyński et al. (2007) concluded that the sequences A, B and C' corresponded to the radial 2nd overtone, first overtone and fundamental modes, respectively, when they used radial pulsation models to try fit the sequences in the period–luminosity (PL) plane at RGB luminosities (see also Dziembowski & Soszyński 2010). This means that the longer period sequence C containing the Miras has no explanation in terms of radial pulsation. This study was extended by Mosser et al. (2013) who matched the A and B sequences at RGB luminosities to sequences of Kepler radial mode pulsators in a PL plane where frequency data was used as a proxy for luminosity. This result produces a close match between sequences B and A and the radial first and second overtones, respectively, in agreement with Soszyński et al. (2007) but not with Wood et al. (1999), Soszyński & Wood (2013) and Takayama, Saio, & Ita (2013). There thus exists two extant assignments of the radial modes to the PL sequences A, B, C' and C that differ by one radial order.

In another study using Kepler data, Stello et al. (2014) showed that in the luminous Kepler red giants, triplets of modes with periods corresponding to spherical degrees $\ell=0$, 2 and 1 (in increasing order of period) are excited for a given radial order. The mode with $\ell=1$ has the largest amplitude for radial orders $n=3$ or more (the second or higher radial overtones). This suggests the OGLE sequences B, A and A' may be dominated by $\ell=1$ modes.

In this paper, the period and luminosity data given in

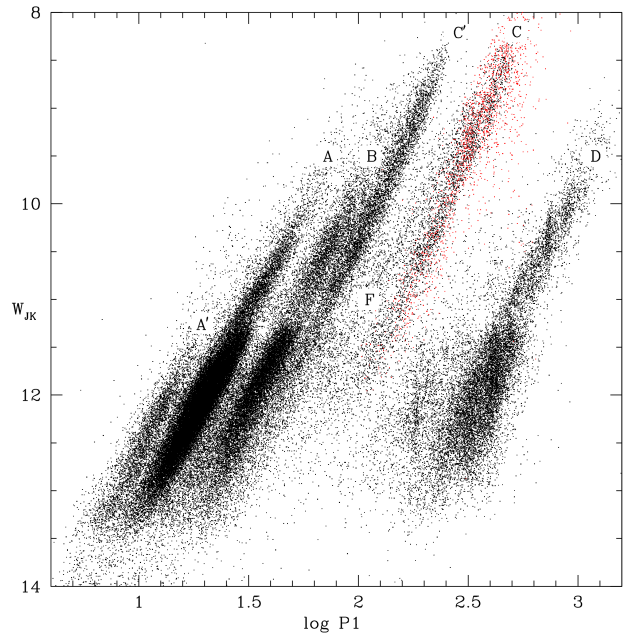


Figure 1. The sequences of variable luminous red giants in the ($W_{JK}, \log P1$) plane, where $P1$ is the period of the mode with the largest amplitude and $W_{JK} = K - 0.686(J - K)$ is a reddening-free measure of the luminosity. Mira variables are shown as red points (in the online version of the paper). The ellipsoidal variables belonging to sequence E are not shown.

the OGLE III catalogue of long-period variables (LPVs) in the LMC (Soszyński et al. 2009) is analysed in detail. Purely empirical results related to the modes, masses and evolution of the stars on the sequences are derived. Then the data are compared to pulsation models in order to throw further light on the modes of pulsation involved.

2 THE SEQUENCES OF LUMINOUS RED GIANTS

The sequences of luminous red giants in the LMC are shown in Figure 1. The period data for this figure come from the OGLE III catalogue of LPVs in the LMC (Soszyński et al. 2009). All the variables in the catalogue are included in the analysis in this paper - no selection is made according to the catalogue types Mira, SRV or OSARG. In the catalogue, three periods are given for each star with the first (or primary) period ($P1$) having the largest amplitude and the secondary periods $P2$ and $P3$ having progressively smaller amplitudes (most luminous red giants exhibit multiple periods of variation). The luminosity in Figure 1 is represented by $W_{JK} = K - 0.686(J - K)$ where the J and K magnitudes are from the 2MASS point source catalogue (Skrutskie et al. 2006). The individual sequences are labelled in Figure 1 although sequence E (produced by the binary ellipsoidal variables) is omitted as these stars are not included in the catalogue. The tip of the RGB is clearly seen at $W_{JK} \sim 11.3$.

The large-amplitude Mira variables are shown as red points in Figure 1. They clearly belong to sequence C. As noted in the Introduction, there are several lines of evidence which suggest that stars on sequence C are fundamental

mode radial pulsators, although some authors have provided arguments against this modal assignment. In Section 7, we will present what we believe to be compelling evidence that the stars on sequence C are indeed fundamental mode pulsators. For these reasons, and to simplify some of the discussion, in this paper it will be assumed from here on that the sequence C stars, including the Mira variables, are fundamental mode radial pulsators.

It is worth considering at this point what causes the existence of the sequences in diagrams like Figure 1. Firstly, remember that the period used in Figure 1 is the primary or largest-amplitude period. At a given luminosity, a star will have possible modes of pulsation with periods that could fall on any of the sequences or (as shall be shown below) between the sequences. The actual position of a star in the figure is determined by the period of the mode of largest amplitude. For self-excited modes, this mode is the one that has the strongest driving - see Soszyński & Wood (2013) for a demonstration of this effect for 1st overtone pulsation on sequence C'. For modes that are excited stochastically by convective motions (solar-like oscillations), there is also a preferred pulsation period which is related to the acoustic cut-off frequency (e.g. Dziembowski et al. 2001; Mosser et al. 2013; Stello et al. 2014).

3 PERIOD RATIOS

Period–luminosity (PL) laws such as those in Figure 1 provide one type of diagram for the comparison of models and observations of variable stars. A more precise diagram for comparing observations and models is the Petersen diagram wherein period ratios in multimode pulsators are plotted against the longer of the two periods in the ratio. In this section, a modified Petersen diagram appropriate for LPVs is discussed.

The upper panel of Figure 2 shows the same PL diagram as Figure 1 but now coloured straight lines have been fitted to each of the pulsation sequences C, C', B, A and A'. It has been assumed that the three sequences B, A and A' have the same slope $dW_{JK}/d\log P1 = 4.444$ while the two sequences C and C' have a slightly different slope $dW_{JK}/d\log P1 = 4.800$.

Since many of the variable LPVs are multimode pulsators, they can be plotted in a Petersen diagram. The lower panel of Figure 2 shows a variant of this diagram where the logarithmic period ratios $\log P2/P1$ and $\log P3/P1$ in each star are plotted against the variable $\log P1[W_{JK}=12]$. The latter quantity is the value of $\log P1$ obtained by projecting the actual value of $\log P1$ along a line parallel to sequence A until it meets the level $W_{JK} = 12$. Specifically, $P1[W_{JK}=12] = \log P1 + (W_{JK} - 12)/4.444$. Stars with primary periods on a given sequence are thus bounded in the same horizontal range in the lower panel of Figure 2, with this range corresponding to the values of $\log P1$ for this sequence when $W_{JK} = 12$. For LPVs, this form of Petersen diagram is much better at revealing preferred period ratios than the traditional Petersen diagram used by Soszyński et al. (2004a) and Takayama, Saio, & Ita (2013) which plots $P_{\text{short}}/P_{\text{long}}$ against P_{long} . A form of Petersen diagram which used a quantity like $P1[W_{JK}=12]$ on the horizontal axis was presented by Soszyński et al. (2007).

The coloured points and short lines in the lower panel of Figure 2 correspond to the ratios of the periods on the fit lines shown in the top panel i.e. they represent the ratios of the periods of the different period–luminosity sequences. The horizontal position of the coloured point/lines is $\log P1[W_{JK}=12]$ for the line which is in the denominator of the period ratio. The colour of the point/line is the colour of the line in the numerator. Coloured points correspond to period ratios of the fits to sequences A', A and B (these all have the same slope). For example, the red point at $(\log P1[W_{JK}=12], \log Pi/P1) \approx (1.12, 0.17)$ represents the ratio of $\log P1$ at the middle of sequence A to $\log P1$ at the middle of sequence A', the red point near $(1.3, 0.0)$ represents this ratio for sequence A to itself and the red point near $(1.52, -0.23)$ represents the ratio for sequence A to sequence B. Since the lines fitted to sequences C and C' have a slightly different slope to that of sequence A, the period ratios of fits involving sequences C or C' lead to the short coloured lines. For example, the short red line at $(\log P1[W_{JK}=12], \log Pi/P1) \approx (1.65, -0.35)$ represents the ratio of $\log P1$ at the middle of sequence A to $\log P1$ at the middle of sequence C'.

We now examine the structure in the lower panel of Figure 2 in detail.

3.1 Observed period ratios for individual stars and for sequences

The black points in the lower panel of Figure 2 show observed period ratios for individual stars. The clustering of these points represents ratios of specific modes present in the data. Firstly, we start with the points in the vertical strip $1.2 \lesssim \log P1[W_{JK}=12] \lesssim 1.4$ which belong to stars with their primary period on sequence A. There is a large cluster of points near $(\log P1[W_{JK}=12], \log Pi/P1) = (1.3, 0.14)$ which one would expect to belong to stars on sequence A that show a secondary period on sequence B. Similarly, the cluster of points near $(\log P1[W_{JK}=12], \log Pi/P1) = (1.3, 0.3)$ should correspond to stars on sequence A that show a secondary period on sequence C' and a third cluster of points near $(\log P1[W_{JK}=12], \log Pi/P1) = (1.3, -0.12)$ which should correspond to stars on sequence A that show a secondary period on sequence A'. However, the period ratio of sequences B, C' and A' to sequence A, represented by the green, magenta and orange points at $\log P1[W_{JK}=12]=1.3$, respectively, do *not* coincide with these clouds of black points. It can be seen that this problem exists for stars with primary periods on any of the sequences. We will explore this situation in detail in Section 4.

Another interesting feature of Figure 2 is that there are clouds of points such as those near $(\log P1[W_{JK}=12], \log Pi/P1) = (1.45, -0.15)$ for which the primary period lies *between* the sequences. One can see in the upper panel of Figure 2 that some stars do have their primary periods between the sequences although they are not as common as the stars on the sequences. In fact, it turns out that the existence of stars between the sequences is related to the problem noted in the previous paragraph and we come back to this in Section 4.

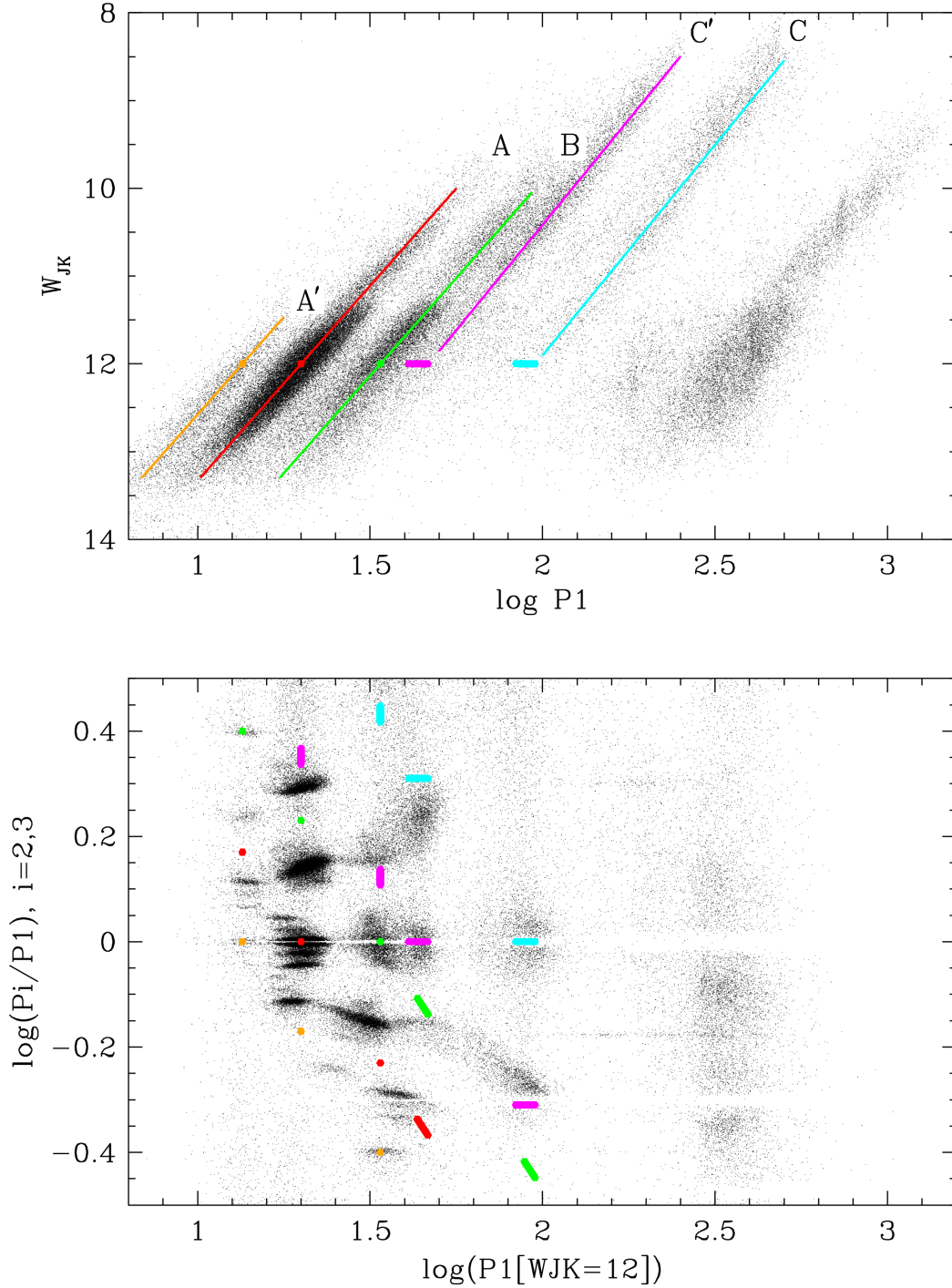


Figure 2. Top panel: The black points show the stars in the $(W_{JK}, \log P1)$ plane while the coloured lines are fits to the sequences. The coloured dots and thick coloured lines are projections of the coloured lines onto $W_{JK} = 12$ along lines of slope $dW_{JK}/d\log P1 = 4.444$. Bottom panel: The black points show the logarithmic period ratios $\log P2/\log P1$ and $\log P3/\log P1$ in individual stars plotted against $\log P1[W_{JK}=12]$ (see text for the definition of this quantity). The coloured points and short lines correspond to the ratios of the periods on the fit lines shown in the upper panel (see text for full details). The colours can be seen in the online version of the paper.

3.2 Closely spaced periods within a sequence

A prominent feature in the lower panel of Figure 2 is the set of sub-ridges first noted by Soszyński et al. (2004a) and especially prominent for stars on sequence A where five almost-horizontal sub-ridges can be seen in the cluster of points

near $(\log P1[W_{JK}=12], \log Pi/P1) = (1.3, 0.0)$. These five sub-ridges must be due to pulsation modes with very closely spaced periods. The spacing is sufficiently small that the individual modes can not be distinguished in a PL diagram such as the top panel of Figure 2. The period separation of low-order radial modes in red giants is much larger than the

Table 1. Stars on the sub-sequences of sequence A

Subgroup	No. of stars	Fraction of sequence A
n(A)	38526	1.000
n(0+1)	639	0.017
n(0+2,2+1)	1152	0.030
n(1+1,2+2,0+0)	10866	0.282
n(1+2,2+0)	2930	0.076
n(1+0)	2754	0.071

period separation of the modes belonging to the five sub-ridges of sequence A so nonradial pulsation modes, as well as a radial pulsation mode, must be involved.

The five sub-ridges of sequence A can be created by three closely-spaced modes each separated in $\log P$ by ~ 0.022 , provided that any of the three modes can be the primary mode in at least some stars. We assume here that this is the case (if one mode was always dominant, five modes would be required). There is some evidence that there are three sub-ridges, corresponding to two close modes, associated with sequence B (see the cluster of points around $(\log P1[W_{JK}=12], \log Pi/P1) = (1.53, 0.0)$). This evidence will be made more apparent in Section 6.

As noted above, the three modes associated with sequence A must include nonradial modes because of their close spacing. We assume that all stars on sequence A, and indeed all stars on any given sequence, have the same radial order of pulsation. Nonradial pulsation models of luminous red giants (e.g. Dziembowski et al. 2001; Mosser et al. 2013; Stello et al. 2014) show that for modes of a given radial order but different angular degree $\ell = 0, 1$ or 2 (the only ones likely to be observed in light curves), the $\ell = 1$ mode has the longest period, the $\ell = 0$ mode has the shortest period and the $\ell = 2$ mode has an intermediate period.

Figure 2 provides a method for determining which of the three modes within sequence A is dominant. Among the stars with their primary period on sequence A' (the points with $1.05 \lesssim \log P1[W_{JK}=12] \lesssim 1.2$), those that also have the closely-spaced modes associated with sequence A can be seen near $(\log P1[W_{JK}=12], \log Pi/P1) = (1.12, 0.12)$. There are three horizontal bands here with the same spacing as the sub-ridges associated with sequence A. The upper band is by far the most prominent. Assuming that one mode dominates sequence A' (because there are no prominent sub-ridges near $(\log P1[W_{JK}=12], \log Pi/P1) = (1.12, 0.0)$), this band structure suggests that it is the longest period mode on sequence A that generally has the largest amplitude. As noted above, this is the $\ell = 1$ mode. The dominance of the $\ell = 1$ mode found on sequence A in the present high luminosity red giants is consistent with the findings of Stello et al. (2014) from Kepler observations but different from that of Mosser et al. (2013) who find the radial $\ell = 0$ mode becomes dominant at high luminosities in their analysis of Kepler stars.

Estimates of the relative amplitudes of the three modes that make up the three sub-sequences of sequence A can be found by examining the populations of the five sub-ridges of sequence A in the Petersen diagram. An exploded view of these sub-ridges is shown in the top panel of Figure 3. Boxes have been drawn to enclose the sub-ridges and the sub-ridges have been named after the possible modes occurring in them.

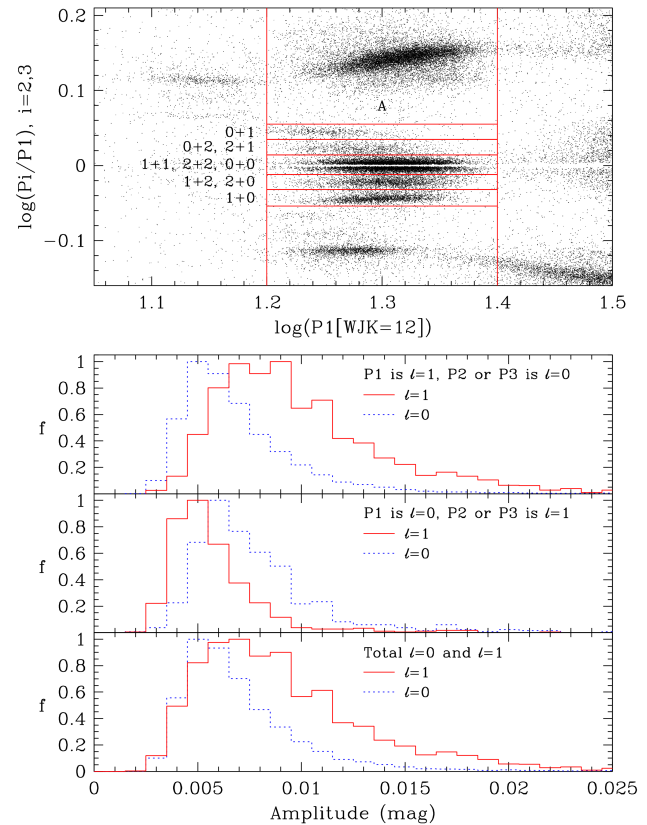


Figure 3. Top panel: The small section of the Petersen diagram containing the five sub-ridges formed by the three pulsation modes forming sequence A. The five boxes enclose the five sub-ridges and their names are shown to the left of the boxes. Bottom panel: The amplitude distribution of the $\ell = 0$ and $\ell = 1$ modes of sequence A when these two modes are present together. See text for further details.

Under our assumption that the three modes involved are the $\ell = 0, 1$ and 2 modes of a single radial order and that the period increases from $\ell = 0$ to 2 to 1 , a star found in the top box must have $\ell = 0$ for its primary period $P1$ and $\ell = 1$ for the secondary period ($P2$ or $P3$). This box has been labelled **0+1**. Similarly, the lowest box **1+0** must have $\ell = 1$ for its primary period $P1$ and $\ell = 0$ for its secondary period. The central box is made up of stars where the same mode is detected twice with slightly different periods and the mode involved could be any of the $\ell = 0, 1$ and 2 modes. The two intermediate boxes are labelled by the possible pairs of modes that could be present. Note that the period separation $\Delta \log P \approx 0.043$ of the $\ell = 0$ and $\ell = 1$ modes obtained from the positions of the sub-ridges agrees with the period separation of these modes given by the observations and the models of Stello et al. (2014), giving added support for the mode identifications.

The fact that the ridges in boxes **0+1** and **1+0** are not strictly parallel to the horizontal axis means that $\Delta \log P$ varies systematically by a small amount across sequence A. Quantitatively, for stars on sequence A, $\Delta \log P$ decreases by ~ 0.0045 as $\log P1[W_{JK}=12]$ increases by 0.1 . An explanation for this behaviour is given in Section 7.2.

The number of stars in each box is given in Table 1.

The total number $n(A)$ of stars with their primary period P_1 on sequence A is also given. This latter number is the total number of stars with $\log P_1[W_{JK}=12]$ lying between the values corresponding to the two vertical lines in Figure 3. Stars that have both the $\ell = 1$ and $\ell = 0$ modes detected in their light curves lie in boxes 1+0 and 0+1. It is clear that $n(0+1)$ is much smaller than $n(1+0)$ which shows that the $\ell = 1$ mode is much more likely to be detected as the *primary* pulsation mode than the $\ell = 0$ mode and this in turn suggests that the $\ell = 1$ mode is likely to have a larger amplitude than the $\ell = 0$ mode. This is shown directly in the bottom panel of Figure 3 where histograms of modal amplitudes are shown (the amplitudes come from the OGLE III catalogue). The top sub-panel shows the amplitudes of the $\ell = 0$ and $\ell = 1$ modes for stars in box 1+0, the middle sub-panel shows the amplitudes for stars in box 0+1 and the bottom sub-panel shows the sum of the top and middle sub-panels. It is clear that the $\ell = 1$ mode tends to have the larger amplitude in stars where the $\ell = 0$ and $\ell = 1$ modes are both present although the non-zero population in box 0+1 shows that the $\ell = 0$ mode can sometimes have a larger amplitude than the $\ell = 1$ mode.

The amplitude distributions shown in Figure 3 apply to stars with two modes on sequence A. However, about 80% of sequence A stars have only one detected mode on sequence A (see the fractions in the last column of Table 1, and note that stars on the middle sub-ridge have two detections of the same mode). Assuming that the relative amplitude distributions shown in Figure 3 are typical, the stars with only a single mode on sequence A will be mostly $\ell = 1$ pulsators, in agreement with the result derived above from the stars that have their primary mode on sequence A' and a secondary mode on sequence A.

One factor that has not been mentioned above is the orientation of the pole of the pulsating star relative to the observer in the case of nonradial pulsation. Different orientations will cause different apparent amplitudes of pulsation for a nonradial pulsator, with a zero apparent amplitude being possible for specific values of ℓ , m and the orientation. As a result, the true numbers of $\ell = 1$ and $\ell = 2$ nonradial pulsators relative to the number of $\ell = 0$ radial pulsators should be higher than indicated by the numbers in Table 1.

4 MULTIPLE MODES IN THE PL DIAGRAM

In Section 3.1 it was shown that period ratios in individual stars do not agree with the period ratios of the mean sequences. A vivid demonstration of this situation is shown in Figure 4. Looking at panel A, it can be seen that the secondary periods form three strips parallel to sequence A, but they are closer to sequence A than are sequences A', B or C'. This situation, wherein the secondary modes are closer to the primary mode than are the adjacent sequences to the central sequence, exists for sequences A', A and C. It also exists for the modes shortward of the primary mode of sequence B and for the mode longward of the primary mode for sequence C'. The only exception to this rule occurs for the mode longward of the primary mode of sequence B (which is further from sequence B than is sequence C') and for the mode shortward of the primary mode of sequence C' (which

is further from sequence C' than is sequence B). We come back to this exception later.

We now seek to explain why the green strips in Figure 4 do not align with the sequences. Firstly, it is assumed here that the pulsation modes that produce the green strips are the same pulsation modes as those that produce the corresponding, neighbouring sequences (where the correspondence is obtained from the ordering in $\log P$ of the strips and sequences). This assumption will be justified in Section 5.1. In this situation, the period of the same mode must be different on a green strip and on its corresponding sequence. Now, in general, the period of a pulsation mode can be written as $P \propto R^\alpha / M^\beta$ where α and β are both positive and for red giants typically range from 1.5–2.3 and 0.5–1.9, respectively (e.g. Fox & Wood 1982). In addition, the position of the giant branch at a given luminosity means that $T_{\text{eff}} = T_{\text{eff}}(L, M)$. Combining these two relations with the definition $L = 4\pi\sigma R^2 T_{\text{eff}}^4$ yields $P = P(L, M)$. Thus if a green strip and its corresponding sequence have the same mode but a different P at a given L then the masses of the stars in the green strip and its corresponding sequence must be different at a given luminosity.

Finally in this section, we return to the exceptional cases of (1) the green strip originating from sequence B which lies on the long period side of sequence C' and (2) the green strip originating from sequence C' which lies on the short period side of sequence B. Remember that in Section 3.2, it was deduced that the $\ell = 1$ mode was the dominant mode in sequence A and that this mode has a period which is ~ 0.043 longer in $\log P$ than the radial mode with $\ell = 0$. Recall also that there appear to be at least two modes (of the same radial order) associated with sequence B. We will show later that these are most likely the $\ell = 1$ and $\ell = 0$ modes, with the former being most common. Finally, as noted in Section 2, stars on sequence C appear to be pulsating in the radial fundamental mode. With these facts in mind, the exceptional cases noted here can be explained naturally if stars on sequences A', A and B are most commonly pulsating in the $\ell = 1$ mode in both their primary pulsation mode and their secondary modes P_2 and P_3 , while stars on sequences C' and C are most commonly pulsating in the radial $\ell = 0$ mode in both their primary pulsation mode and their secondary modes. Thus the stars with primary modes on sequence B will have $\log P$ for their secondary modes increased relative to $\log P$ of the radial mode pulsators on sequence C' by $\Delta \log P \sim 0.043$, thereby causing the exceptions noted in points (1) and (2) above. Note that the offset $\Delta \log P \sim 0.043$ is derived from the populous RGB. Since the slope of sequences C and C' is steeper than the slope of sequences A', A and B, this offset will increase with luminosity and will be larger for AGB stars.

An alternative explanation for the exceptional cases would be for the stellar mass to decrease from sequence A' to A to B, then to increase to sequence C' then decrease again to C. This seems contrived and is not consistent with the evolutionary picture described in the next section.

4.1 The stars on sequence D

Although generally not part of this study, in the last panel of Figure 4 the secondary periods of stars with their primary period on sequence D are shown as green points. This plot

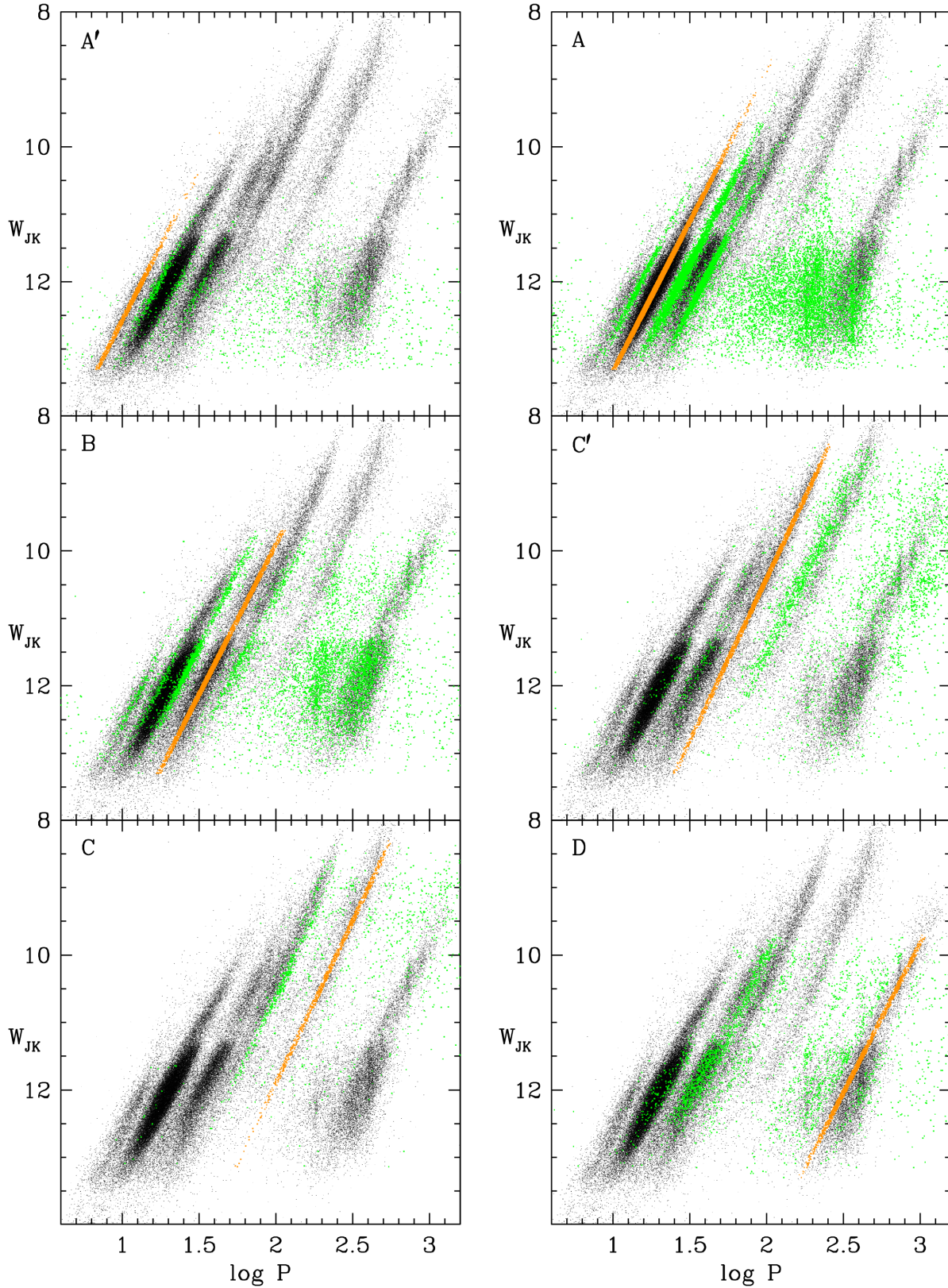


Figure 4. Plots of W_{JK} against the primary period P_1 for stars in the OGLE III catalogue (black points). Each panel is labelled by a sequence name and the stars with primary periods lying in a channel running along the centre of the named sequence have been plotted as orange points. Secondary periods P_2 and P_3 for the stars with P_1 in the orange channel are plotted as green points. For clarity, green points close to the orange channel are not plotted: the excluded points have $|\log P_2 - \log P_c| < 0.07$ and $|\log P_3 - \log P_c| < 0.07$, where $\log P_c$ is $\log P$ at the centre of the channel. The excluded points are second detections of the mode represented by the orange points. The colours can be seen in the online version of the paper.

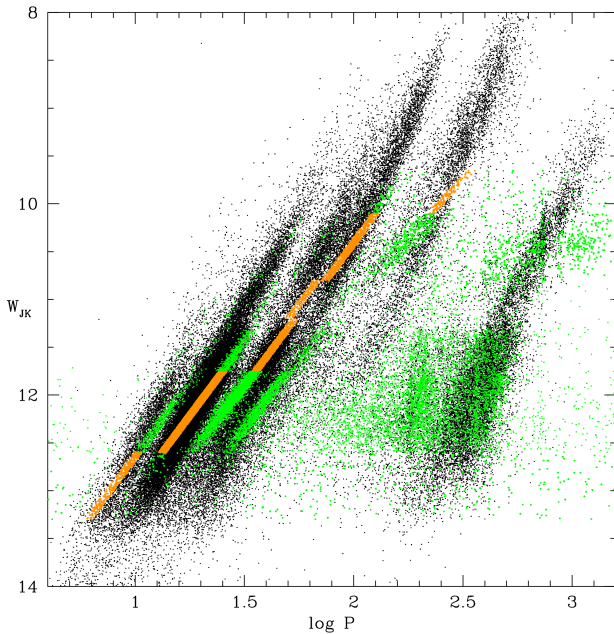


Figure 5. Plots of W_{JK} against the primary period P_1 for stars in the OGLE III catalogue (black points). Evolutionary channels cross each sequence from left to right and stars whose primary periods fall in these channels are plotted as orange points. The secondary periods P_2 and P_3 of the stars with P_1 in the orange channels are plotted as green points. See text for further details. The colours can be seen in the online version of the paper.

highlights the fact that the periods of pulsation associated with the LSPs of sequence D lie mainly on or near sequence B.

4.2 The stars on sequence F

The faint sequence F between sequences C' and C is marked in Figure 1. In panel C' of Figure 4, it can be seen that secondary periods of stars whose primary period lies on sequence C' form a sequence close to sequence F. This suggests that the sequence F stars are possibly fundamental mode pulsators like the stars on sequence C. However, it is not clear why the sequence F stars should form a distinct sequence. One possible explanation is that they are high mass LPVs (so that their periods are shorter than the periods typical of sequence C stars) formed in a relatively recent burst of star formation.

5 THE EVOLUTION OF LPVS

5.1 Tracks in the PL diagram

For most of the stars in PL diagrams such as Figure 1, mass loss is small so that the evolutionary track of a star is represented by a line of constant mass and pulsation mode. An examination of pulsation models shows that in the $(W_{JK}, \log P)$ plane, lines of constant mass and pulsation mode have a smaller slope than the sequences (e.g. Soszyński & Wood 2013). In Figure 5, channels similar to those in Figure 4 have been drawn but now the channels are roughly parallel to lines of constant mass and pulsation mode so

they represent evolutionary tracks. The slopes of the tracks are estimated from the pulsation models described in Section 7. For convenience of plotting, at lower luminosities on sequences A' , A and B, the orange channels have been drawn more tilted relative to the sequences than the models indicate but this does not qualitatively affect the empirical evolutionary scheme presented here.

Consider stars in Figure 5 whose primary period lies in the orange strip through sequence A. As stars in this channel evolve to higher luminosity, they slowly move from the short period side of sequence A to the long period side. At the same time, there is a declining prominence of the secondary period corresponding to the next highest radial order (the green strip to the left of the orange channel in sequence A) and an increasing prominence of the secondary period corresponding to the next lowest radial order (the green strip to the right of the orange channel in sequence A). This means that the primary period most likely detected by observations will move to a lower radial order as the luminosity increases. Thus the orange points representing the evolving stars in Figure 5 will jump from the long period side of sequence A to the short period side of sequence B because the highest amplitude mode has moved from that associated with sequence A to that associated with sequence B. Evolution will then continue up and across sequence B before a jump to sequence C' and so on. Note that in the empirical scheme shown here, the point of transition of the orange channels from sequence to sequence is judged by eye since current pulsation models do not give reliable theoretical estimates of mode amplitudes.

When a star reaches the RGB tip, it will transit to a lower-luminosity core-helium burning phase before rising again up the AGB with a slightly shorter period than it had at the same luminosity on the RGB. This situation is shown in Figure 5 for the stars in the channel on sequence B. The AGB evolution is shown only after the RGB tip luminosity ($W_{JK} \sim 11.3$) is exceeded.

5.2 Mass variations through the sequences

The evolutionary scenario described in the previous subsection has implications for the masses of stars on the sequences. Note firstly that, on a given sequence, stars of different mass will follow essentially parallel tracks but the higher mass stars will be found at higher luminosities. This means that the mass increases up a sequence, it increases to shorter periods across a sequence at a given luminosity, and it also increases from sequence to sequence at a given luminosity as the radial order increases (the sequence period decreases). Note that a mass difference between sequences was invoked above in order to explain why the period ratios between the sequences did not match the period ratios in individual stars. The evolutionary scenario provides an understanding for this empirical finding.

The periods of stars in the various sequences formed in PL diagrams by using the primary or secondary periods can be used to estimate the mass variation from sequence to sequence and the mass variation across sequences. Figure 6 shows a histogram of the number of stars in a horizontal band defined by $W_{JK} = 12 \pm 0.25$ in panel A of Figure 4. Here we are interested in exploring the mass variation from sequence B to sequence A and the mass varia-

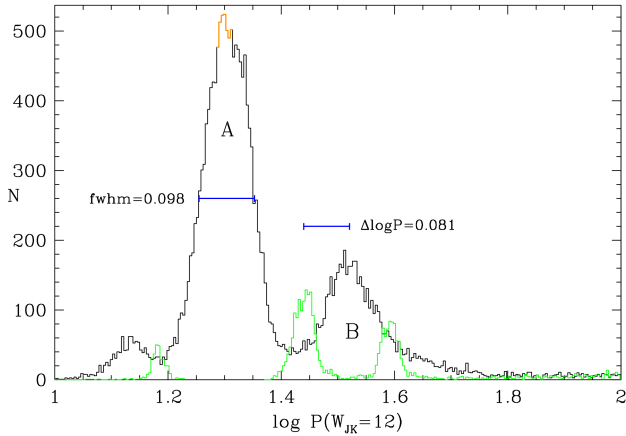


Figure 6. Histogram of the number of stars in a horizontal band defined by $W_{JK} = 12 \pm 0.25$ in panel A of Figure 4. The horizontal position of each star is given by the value of its coordinate $\log P[W_{JK}=12]$. The black curve is obtained by using the primary period $P1$ of each star. The orange segment of this curve represents the sequence A stars in the orange channel through the middle of sequence A. The green curve is obtained by using the secondary periods $P2$ and $P3$ of those stars in the orange channel (i.e. this is the histogram of the green points in panel A of Figure 4). The colours can be seen in the online version of the paper.

tion across sequence A. The positions of sequences A and B are marked on Figure 6. The peak in the green distribution at $\log P[W_{JK}=12] \approx 1.44$ is formed by sequence A stars whose secondary periods are produced by the pulsation mode which produces sequence B. The difference $\Delta \log P \sim 0.081$ in the positions of this peak and the sequence B peak is caused by the different masses of stars on sequences A and B. Pulsation models for low radial order modes at the luminosities and masses of the stars involved here show that, at a given luminosity, $P \propto M^{-0.8}$ (this result comes from the pulsation models described in Section 7). Thus the shift $\Delta \log P \sim 0.081$ corresponds to the average mass of stars on sequence A being approximately 26% larger than the average mass of stars on sequence B.

Mass variations *within* a sequence are also required. These mass variations make a large contribution to the finite width in $\log P$ of the sequences, with the mass increasing to shorter periods across the sequences. Let us consider sequence A. The total width of this sequence (represented by the full-width at half maximum) is $\Delta \log P \sim 0.098$. As well as the mass variation across the sequence, there is also a contribution to the sequence width from the period variability represented by the vertical width of the sub-ridges in the top panel of Figure 3. This contributes approximately $\Delta \log P \sim 0.01$ to the observed width of sequence A, leaving the contribution from mass variation alone at $\Delta \log P \sim 0.088$. The sub-sequences of sequence A (i.e. the multiple modes) will also make a small contribution to the width but we ignore this. The width $\Delta \log P \sim 0.088$ means that the mass increases by about 29% from the longer period to the shorter period side of sequence A.

In the evolutionary scenario described above, the mass variation across a sequence should be equal to the mass variation between sequences. Remember that stars jump be-

tween sequences from the long period edge of one to the short period edge of the other. Thus the masses of stars on the long period side of a sequence should be the same as the masses of stars on the short period edge of the adjacent longer period sequence. Consequently, the mass difference between the short period edges of two adjacent sequences will be the mass difference across the shorter period sequence. The results given above for sequences A and B show that the mass difference between these two sequences is indeed close to the mass difference across sequence A.

The procedure applied above to determine the difference in the average masses of stars on sequences A and B can be applied to other pairs of sequences in which stars pulsate mostly in the same mode. We find that stars on sequence A' are $\sim 17\%$ more massive than stars on sequence A at luminosities around $W_{JK} = 12$. The difference in the average masses of stars on sequences C' and C cannot be readily determined at this luminosity since the mode of sequence C is rarely seen there. However, near $W_{JK} = 10.5$, which is on the AGB, many stars exhibit primary and secondary oscillations in both of the modes associated with sequences C' and C. The period shifts indicate that the stars on sequence C' are $\sim 16\%$ more massive than those on sequence C. To derive this result we used the formula $P \propto M^{-1.1}$ rather than $P \propto M^{-0.8}$ which is appropriate at lower luminosities on the RGB (these formulae are derived from the pulsation models described in Section 7). Finally, we consider sequences B and C'. Comparing the masses of stars on these two sequences is difficult at any luminosity because of the paucity of stars that exhibit both the sequence B and C' modes, and because the stars with primary periods on sequence B appear to be $\ell = 1$ pulsators while stars with primary periods on sequence C' appear to be $\ell = 0$ pulsators. We do not make any estimate of the mass difference between these two sequences.

6 THE LUMINOSITY DEPENDENCE OF PERIOD RATIOS

Although Figure 2 demonstrates the existence of secondary periods in many LPVs, it does not indicate how the presence of secondary periods varies with luminosity. The luminosity dependence of the secondary periods can be seen in Figure 7. For each sequence, this figure plots W_{JK} against the secondary period relative to the primary period whose position is marked by a vertical blue line. The vertical strips of black points show where individual secondary modes are present in the stars. The radial order of the modes associated with these secondary modes are indicated by coloured numbers, with radial order 1 corresponding to the fundamental mode (see Section 7 for the justification of the assignment of radial orders). The positions of the individual sequences are indicated by coloured dots in each panel. The fact that the dots and numbers of the same colour do not align horizontally (except for the reference mode) is yet another demonstration of the fact that the ratio of the periods in individual stars do not match the ratio of the periods of the sequences.

Panel A' of Figure 7 shows the ratio of secondary to primary period for stars whose primary period lies on sequence A'. Looking at this panel, we see three closely-spaced vertical bands under and slightly left of the red 4. These bands

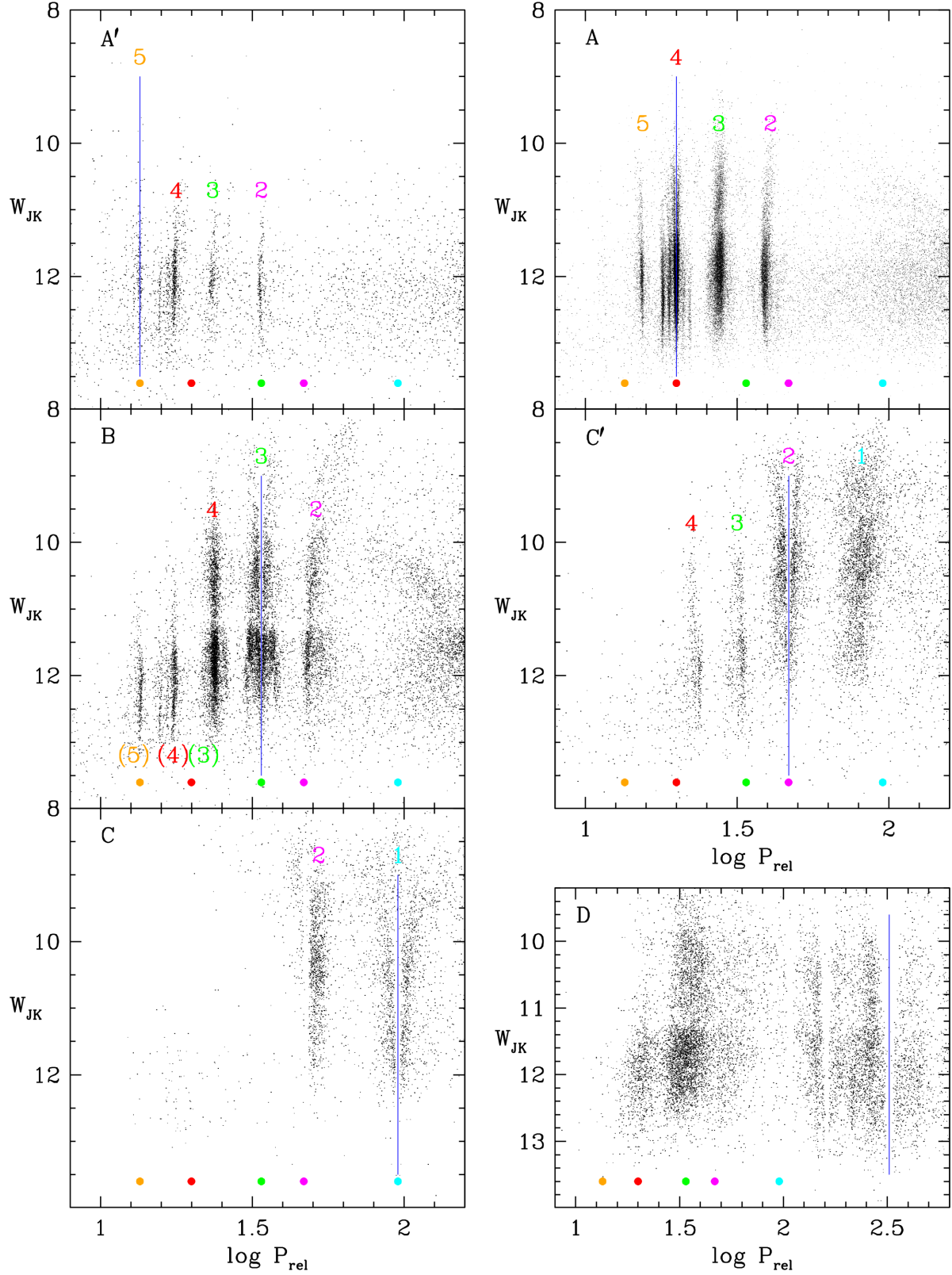


Figure 7. W_{JK} plotted against the ratio of secondary period to the primary period for stars whose primary periods lie in a strip of width $\Delta \log P_1 = 0.12$ down the centre of each sequence. Here $\log P_{\text{rel}}$ is defined as $\log P_{\text{rel}} = \log(P_2/P_1) + \log P_{\text{centre}}$ or $\log P_{\text{rel}} = \log(P_3/P_1) + \log P_{\text{centre}}$, where $\log P_{\text{centre}}$ is $\log P$ at the centre of the sequence when $W_{JK} = 12$. The blue vertical line in the panel for each sequence is situated at $\log P_{\text{centre}}$. The coloured dots indicate $\log P_{\text{centre}}$ for each sequence using the colour coding for the sequences adopted in Figure 2. The coloured numbers count the observed radial orders in each panel and these numbers are aligned consistently from panel to panel, starting at 1 for the mode with the longest observed period in panel C. The colours can be seen in the online version of the paper.

are caused by the three modes occurring on sequence A. The longest period mode (the $\ell = 1$ mode) becomes dominant as the luminosity increases. This result is also seen for stars with their primary period on sequence A (see panel A). There are five vertical bands associated with sequence A and these are caused by the three modes present within this sequence. As discussed in Section 3.2, the shortest period band is produced by stars whose primary mode has $\ell = 1$ and whose secondary mode has $\ell = 0$ while the longest period band is produced by stars whose primary mode has $\ell = 0$ and whose secondary mode has $\ell = 1$. The shortest period band extends to higher luminosities than the longest period band which suggests that the $\ell = 1$ mode is more prominent as the primary period (i.e. the one with largest amplitude) at higher luminosities. Once again, we note that the dominance of the $\ell = 1$ mode at higher luminosities on sequence A is consistent with the findings of Stello et al. (2014) from Kepler observations but different from the findings of Mosser et al. (2013) who suggest that the radial $\ell = 0$ mode becomes dominant at high luminosities.

The stars with their primary mode on sequence B show three¹ vertical bands associated with the primary mode (panel B of Figure 7). This structure indicates the presence of two close modes but they seem to be confined to RGB stars only ($W_{JK} > 11.3$). Only one mode appears to be present on the AGB.

Panel B in Figure 7 reveals the presence of apparent extra modes not present in any other panel. In a simple sequential assignment of radial orders, there appear to be secondary modes present corresponding to radial orders 5 and 6. However, looking at panel A' immediately above panel B, it can be seen that the mode structure associated with the radial orders 4 and 5 in panel A' is reproduced exactly in panel B. Another point to notice is that the horizontal position of radial order 2 in panel A' coincides exactly with the position of sequence B. We conclude from these facts that stars whose primary mode lies on sequence B are of two types: (1) stars pulsating in the third radial order with secondary periods in the second and fourth radial orders, and (2) stars pulsating in the second radial order with secondary periods in the third, fourth and fifth radial orders. The type 2 stars are more massive than type 1 stars and they have masses typical of stars on sequence A'. These type 2 stars are really stars belonging to sequence A' but the observed amplitude of the radial order 2 pulsations is larger than the observed amplitude of the radial order 5 pulsations so they end up on sequence B. The apparent extra radial orders in panel B have been labelled by their true radial orders using numbers in brackets.

If we consider the stars on sequence B whose primary mode is of radial order 3 (panel B of Figure 7), we see that the secondary modes pulsating in radial order 4 form two bands with the shorter period band being overwhelmingly dominant (the apparent band on the short period side of the radial order 4 group belongs to radial order 3 of the type 2 stars examined in the last paragraph). Given that there are

two possible primary modes of radial order 3, the dominance of the shorter period band in panel B suggests that the dominant primary mode is the longer period one. The separation $\Delta \log P \approx 0.04$ of the two modes associated with radial order 3 (derived from the separation of the vertical bands associated with this order in panel B of Figure 7) is consistent with the separation of the $\ell = 0$ and the $\ell = 1$ modes of radial order 3 in the models of Stello et al. (2014). These results therefore suggest that the $\ell = 0$ and the $\ell = 1$ modes are present on sequence B and that the $\ell = 1$ mode is dominant. The direct finding that the $\ell = 1$ mode is dominant on both sequences B and A is consistent with the suggestion in Section 4 that the $\ell = 1$ mode is dominant on each of sequences B, A and A'.

7 COMPARISON OF OBSERVATIONS AND RADIAL PULSATION MODELS

In this section, period ratios observed in individual stars are compared to period ratios in radial pulsation models of red giants. The linear, non-adiabatic pulsation models were computed with the code described in Wood & Olivier (2014) using the same input parameters (abundances, mixing-length, turbulent viscosity parameter, core mass) as in that paper. Evidence was presented in Section 4 that, in a given star, both the dominant primary pulsations and the secondary pulsations correspond to modes of the same spherical degree ℓ . Thus, although the nonradial $\ell = 1$ mode appears to dominate the primary pulsations in sequences A', A and B, provided the ratio of the $\ell = 1$ to the $\ell = 0$ periods is approximately the same for radial orders 3 to 5 associated with these sequences, the observed period ratios in individual stars should be the same as the period ratios in radial pulsation models. In Figures 8 and 9 the observed period ratios in individual stars are compared to the period ratios in radial pulsation models.

In Figure 8, it is assumed that the radial mode associated with sequence C (the Mira sequence) is the fundamental mode (radial order 1) and that sequences C', B, A and A' correspond to successively higher radial orders of pulsation. It can be seen that for each of the panels in Figure 8, the model period ratios match the observed period ratios well for some mass in the range 0.8 to $2.4 M_{\odot}$ except for the highest mass and luminosity models in panels C' and C. This problem is discussed in Section 7.3. Note that in panel B, there is a mismatch between the models and those vertical bands that really belong to sequence A' (as described in Section 6) but this is expected because of the different masses of stars on sequences A' and B. Overall, these results provide strong evidence that the primary pulsation modes associated with sequences C, C', B, A and A' belong to radial orders 1, 2, 3, 4 and 5. It also provides strong evidence that both primary and secondary pulsations in a given star tend to belong to the same ℓ value.

In Figure 9, it is assumed that the radial mode associated with sequence C' is the fundamental mode (radial order 1) and that sequences B, A and A' correspond to successively higher radial orders. Clearly, the mode marked by the cyan number 1 (sequence C) has no explanation in terms of radial modes with this assignment of radial orders. Furthermore, even for higher radial orders, the ratios of mode

¹ The apparent splitting near $W_{JK} = 12$ of the outer bands of sequence B are caused by the 1-year alias of the primary period, so this feature is not real. A similar 1-year alias can be seen in the bands of sequence A near $W_{JK} = 11.2$ if the figure is expanded.

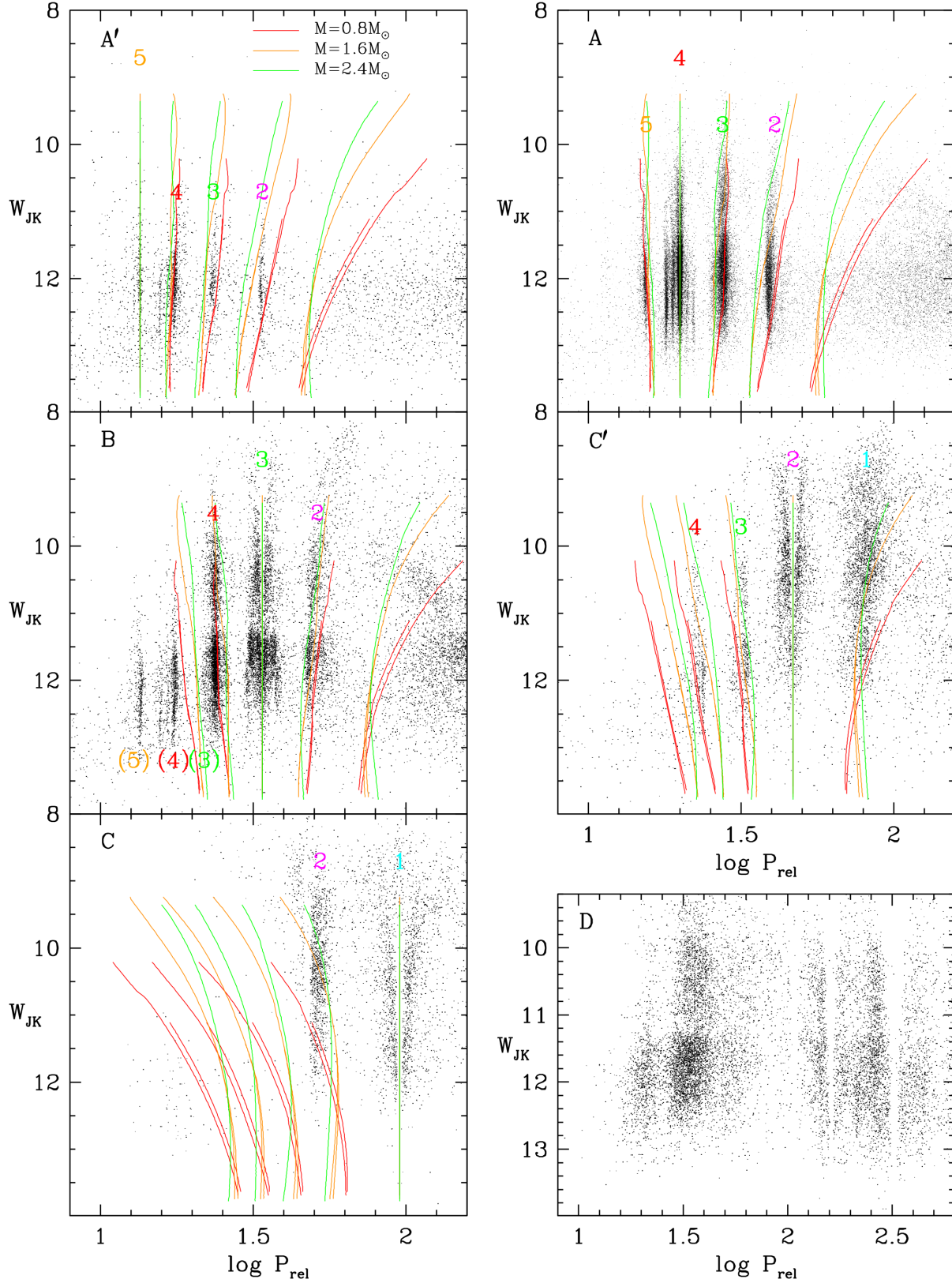


Figure 8. Same as Figure 7 with the addition of radial pulsation models showing the logarithmic period ratios for the first five modes. It is assumed that sequence C corresponds to the fundamental mode (radial order 1) and that sequences C' to A' correspond to the first to fourth overtone (radial orders 2 to 5), respectively. In each panel, the model period ratios are taken relative to the radial order appropriate for the sequence assigned to the panel. Models with masses of 0.8, 1.6 and $2.4 M_{\odot}$ are represented by red, orange and green lines, respectively. Both AGB and RGB models are plotted for M equal to 0.8 and $1.6 M_{\odot}$ (there is no RGB for $M = 2.4 M_{\odot}$). The AGB and RGB models are only separable for the fundamental mode. The colours can be seen in the online version of the paper.

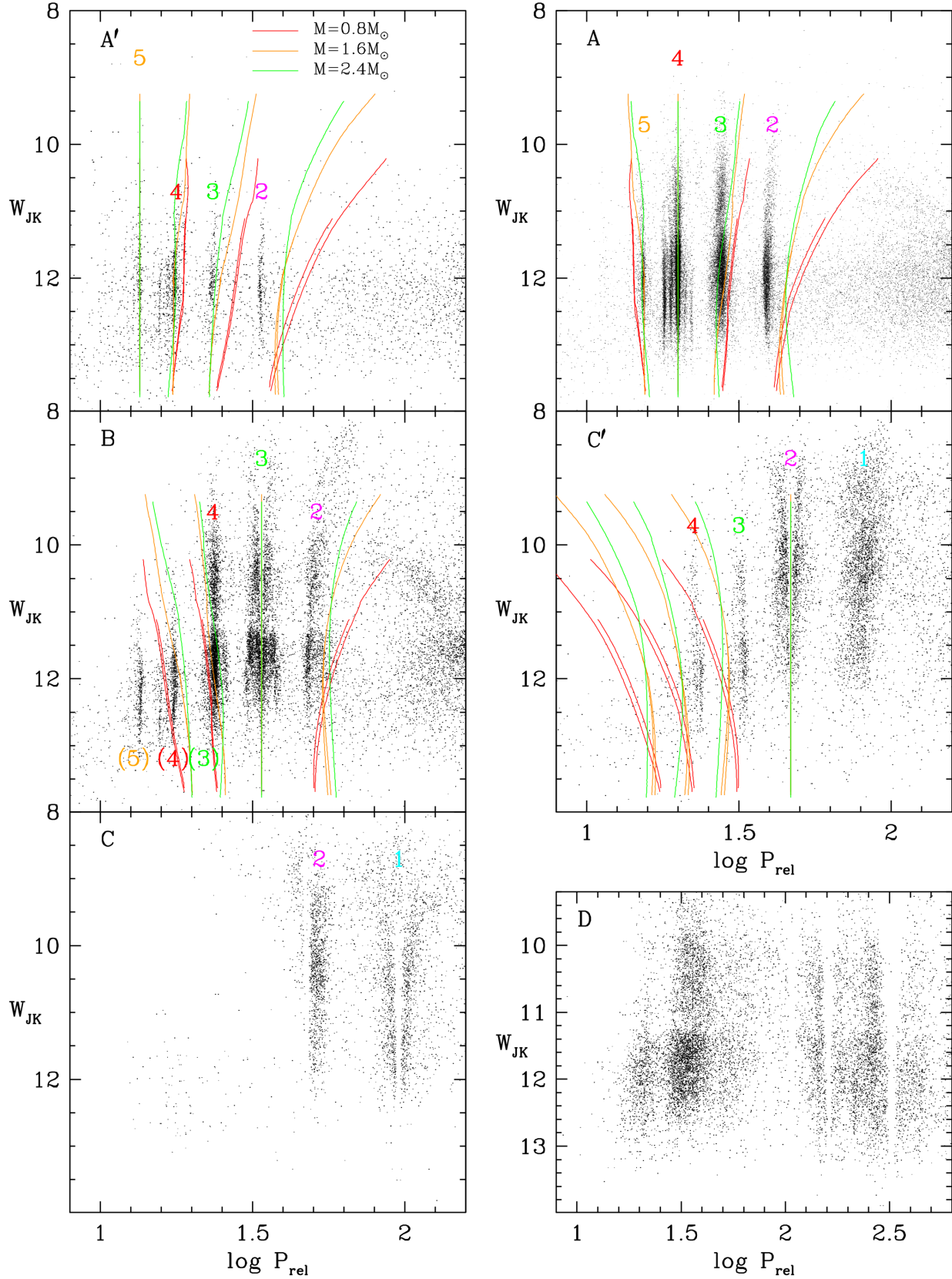


Figure 9. Same as Figure 8 but now it is assumed that sequence C' corresponds to the fundamental mode (radial order 1) and that sequences B, A and A' correspond to the first to third overtone (radial orders 2 to 4), respectively. Only the first four radial modes of the models are shown.

periods in the models fail to match the observed ratios. We therefore reject this modal assignment.

7.1 Comparison with previous modal assignments

The finding here that sequences C, C', B, A and A' correspond to radial orders 1, 2, 3, 4 and 5 is consistent with most earlier findings (e.g. Wood & Sebo 1996; Wood et al. 1999; Takayama, Saio, & Ita 2013). However, this assignment is inconsistent with the suggestion of Soszyński et al. (2007) and Mosser et al. (2013) that sequence C' corresponds to radial order 1.

In terms of nonradial modes, we find direct evidence for the presence of the $\ell = 1$ mode on sequences A and B and for the $\ell = 2$ mode on sequence A. In their analysis of OGLE III data, Takayama, Saio, & Ita (2013) claim to find the presence of the two nonradial modes. Firstly, they associate the $\ell = 2$ mode of radial order three² with sequence B while the only nonradial mode we find has $\ell = 1$. Secondly, they find the $\ell = 1$ mode of radial order 5 associated with sequence A whereas we associate radial order 5 with sequence A' and we find the $\ell = 1$ mode of radial order 4 associated with sequence A. Because Takayama, Saio, & Ita (2013) only looked at LPVs on the RGB designated as OSARGS in the OGLE III catalogue, all LPVs with periods on sequences A' and C were excluded (by definition, OSARGS on the RGB do not have these modes) so they had an incomplete picture of the modes involved. In addition, the Petersen diagram they used meant that a number of modes overlapped on the figure causing confusion.

7.2 The mass dependence of the period ratios

In the lower panel of Figure 2, the various clusters of points representing period ratios of specific pairs of modes tend to form ridges that are not horizontal. For example, we now know that the ridge at $(\log P1[W_{JK}=12], \log P_i/P1) \approx (1.3, 0.3)$ corresponds to stars whose primary pulsation mode belongs to radial order 4 and whose secondary pulsation mode belongs to radial order 2. This group of points, and most of the other groups of points, form ridges such that the period ratio becomes smaller when moving from the long period side of the primary mode sequence to the short period side. It was shown in Section 5.2 that the mass of stars in a sequence increases when moving from the long period side to the short period side of the sequence. This suggests that the cause of the non-zero slope of the ridges in the lower panel of Figure 2 is mass variation across sequences. The models shown in Figure 8 confirm this. If we take the example given above for the ridge at $(\log P1[W_{JK}=12], \log P_i/P1) \approx (1.3, 0.3)$, panel A of Figure 8 shows that the period ratio of radial order 2 to radial order 4 modes decreases as the model mass increases, just as suggested by the slope of the ridges.

It was noted in Section 3.2 that the ratio of the periods of the $\ell = 1$ and $\ell = 0$ modes of radial order 4 increased slightly from the long period side to the short period side

² Takayama, Saio, & Ita (2013) use a nomenclature in which the radial order is offset by one from the nomenclature used here. For example, their p -mode p_2 corresponds to radial order 3 in this paper.

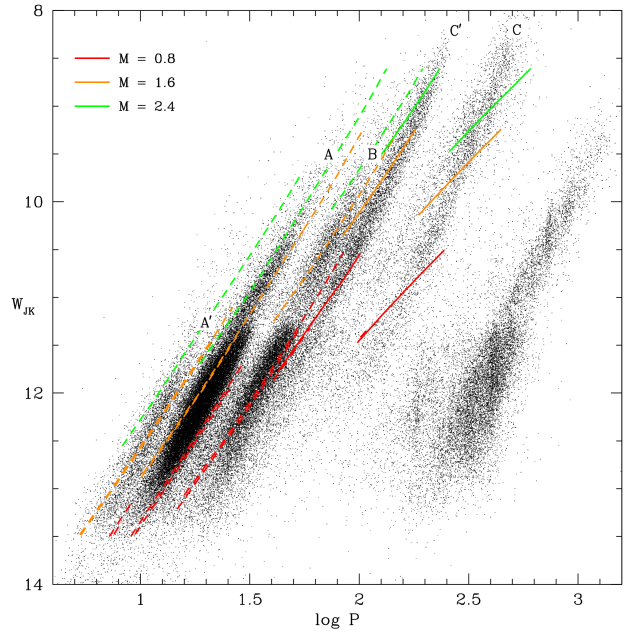


Figure 10. Plots of W_{JK} against the primary period $P1$ for stars in the OGLE III catalogue (black points). The coloured lines show the positions of modes from the first five radial orders for stars of mass 0.8, 1.6 and $2.4 M_{\odot}$. The lines for each mode are plotted only in regions where they cross the sequence in which the mode is expected to dominate. The first two radial orders are shown as continuous lines and they correspond to the fundamental and first overtone radial pulsation modes. The lines for the next three radial orders are shown as dotted lines because the periods shown have been increased by $\Delta \log P = 0.043$ from the period of the radial modes in an attempt to simulate the periods of the $\ell = 1$ pulsation mode. The colours can be seen in the online version of the paper.

of sequence A (the opposite slope to the cases considered in the previous paragraph). This result provides evidence for the mass dependence of the period ratio of the $\ell = 1$ and $\ell = 0$ modes, with the period ratio increasing with mass. Combining the results for the variation of the period ratio across sequence A from Section 3.2 with the results for the variation of mass across sequence A from Section 5.2, we find that $\partial \log(P(\ell = 1)/P(\ell = 0))/\partial \log M \approx 0.036$ for the stars on sequence A. This result provides a test for nonradial pulsation models of luminous red giant stars.

7.3 Pulsation masses from the models

Until now in this paper, only period ratios have been compared to models because period ratios are less sensitive to model parameters than are the periods themselves. In addition, to compare model and observed periods in (say) the $(W_{JK}, \log P)$ plane, conversions from model T_{eff} and L to the observed W_{JK} are required. These conversions are not particularly well known for cool stars such as LPVs and there are additional problems due to interstellar and circumstellar reddening and the distance modulus (although the latter is now well-determined for the LMC). Keeping these problems in mind, in this final sub-section, we do compare the models to the observations in the $(W_{JK}, \log P)$ plane.

For each stellar model, T_{eff} and L have been converted

to J and K in the 2MASS system using the tabulated bolometric corrections obtained from the model atmosphere calculation by Houdashelt et al. (2000) and Houdashelt, Bell, & Sweigart (2000) for a metal abundance $[\text{Fe}/\text{H}] = -0.5$ which is appropriate for the LMC and which is consistent with the metal abundance used in the model calculations. Conversion of J and K in the system of Houdashelt et al. (2000) and Houdashelt, Bell, & Sweigart (2000) to the 2MASS system is done using the conversions in Carpenter (2001). An LMC distance modulus of 18.54 and a reddening $E(B - V)$ of 0.08 from Keller & Wood (2006) are used, along with the reddening law of Cardelli, Clayton, & Mathis (1989) to get the reddening at J and K .

Figure 10 is a plot in the $(W_{\text{JK}}, \log P)$ plane of the periods and luminosities of modes from the first five radial orders of stars with masses of 0.8, 1.6 and 2.4 M_{\odot} . For each mode, only a short line segment is plotted centred on the position where it crosses the sequence in which the mode is assumed to be dominant. Note that the models computed here only produce periods for radial modes. However, it was shown in Sections 4 and 6 that the $\ell = 1$ mode is dominant on sequences A' , A and B , and in Section 7 it was shown that these sequences correspond to radial orders 5, 4 and 3, respectively. Furthermore, in Sections 3.2 and 4 it was shown that the period of the $\ell = 1$ mode is longer than the period of the $\ell = 0$ mode by $\Delta \log P \approx 0.043$. Hence, to compare the models with the observations, the computed periods for radial orders 3, 4 and 5 have been increased by $\Delta \log P = 0.043$ before being plotted in Figure 10. This correction is made in order to simulate the $\ell = 1$ mode periods. The resulting periods are shown in Figure 10 by dashed lines.

We now make a detailed comparison of the models with the observations. Looking at sequence C in Figure 10, it can be seen that fundamental mode pulsation in stars with masses in the range 0.8–2.4 M_{\odot} explains most of these stars, with some stars outside this mass range required to explain the full length of the sequence (note that the present-day population of red giant stars in the LMC peaks at masses around 1.6 M_{\odot} e.g. Nie, Wood, & Nicholls 2012). Stars in a similar mass range, but pulsating in the radial first overtone mode can explain the stars on sequence C' . Similarly, this mass range fits sequences B , A and A' but at lower luminosities, as expected from the empirical evolution scheme described in Section 5.1. The mass required to fit these three sequences at a given luminosity increases when moving from sequence B to A to A' , consistent with the results derived in Section 5.2 from the empirical evolution scheme. In addition, the width of sequence A requires a significant range of masses to be present at a given luminosity. This is also consistent with the results derived in Section 5.2. Given the various results presented in this paragraph, there appears to be reasonable agreement between the models and the observations in the $(W_{\text{JK}}, \log P)$ plane in spite of the potential difficulties mentioned above.

There is one parameter on which the models and the empirical evolution scheme are in relatively poor agreement. This is the transition luminosity at which stars move from one sequence to the next, especially in the case of the transition from sequence C' to sequence C . Looking at the evolutionary track for a 1.6 M_{\odot} star (i.e. the orange lines in Figure 10), we see that the first overtone mode does not cross

the long period edge of sequence C' until $W_{\text{JK}} \sim 9$. According to the empirical evolution scheme, the star should then jump to the short period edge of sequence C and start pulsating in the fundamental mode at $W_{\text{JK}} \sim 9$. However, the period of the fundamental mode of the 1.6 M_{\odot} star at this stage puts the star at the *long* period edge of sequence C or beyond. This suggests that the ratio of the fundamental to first overtone periods in the models is too large. Actually, the disagreement between the models and the observations is not as bad as just suggested. If we look at panel C' of Figure 8, we see that the logarithmic period difference $\Delta \log P$ between the fundamental mode to the first overtone mode is ~ 0.26 around $W_{\text{JK}} \sim 9 - 10$. This is significantly larger than the difference $\Delta \log P \sim 0.18$ between the long period edge of sequence C' and the short period edge of sequence C . At $W_{\text{JK}} = 10$, $\Delta \log P$ for the 1.6 M_{\odot} star is indeed ~ 0.26 but by $W_{\text{JK}} = 9$ $\Delta \log P$ is much too large at ~ 0.41 so that there is still a discrepancy between the model period ratios for the first two modes and the observed ratio of these two modes. It is worth noting that the discrepancy discussed here seems to be worst at high masses and luminosities. At $M = 0.8 M_{\odot}$, the models predict a transition from the long period edge of sequence C' to the short period edge of sequence C which is as predicted by the empirical evolution scheme.

Finally, we take a look at the period difference between RGB and AGB stars. The lines drawn in Figure 10 belong to both RGB and AGB stars. The computed separation of the RGB and AGB periods for each mode at a given luminosity is almost imperceptible on the plot (the separation can just be seen for the 0.8 M_{\odot} models). It is certainly much less than the period shift of $\Delta \log P \sim 0.05$ evident on sequence A when moving from the RGB at $W_{\text{JK}} > 11.3$ to the AGB at $W_{\text{JK}} < 11.3$. The observed period shift can not be explained by mass loss between the RGB tip and the AGB since mass loss increases the period of pulsation whereas the period is observed to decrease. The models thus predict that there is a very small period change between the RGB to the AGB for a given mode. A possible interpretation of the much larger period shift observed on sequence A when going from the RGB to the AGB is that the AGB is dominated by radial ($\ell = 0$) pulsators while the RGB is dominated by nonradial $\ell = 1$ pulsators (remember that $\Delta \log P \sim 0.043$ for the period ratio of the $\ell = 1$ and $\ell = 0$ modes). However, this result conflicts with the results in Section 6 which suggested that the $\ell = 1$ mode becomes more dominant at higher luminosity. The observational resolution of this conflict awaits larger data sets such as those that will come from OGLE IV.

8 SUMMARY AND CONCLUSIONS

Multiple pulsation modes in stars in the OGLE III catalogue of LPVs in the LMC have been examined. It has been shown that the ratios of the multiple periods in individual stars do not agree with the ratios of the periods of the sequences of LPVs in the PL diagram. This leads to the conclusion that the average masses of stars on the different sequences vary, with the shorter period sequences containing more massive stars. An examination of the evolution of stars in the PL diagram shows that the mass variation between sequences is the same as the mass variation across individual sequences.

As an example, it is shown that the average mass of a star on sequence A is $\sim 26\%$ higher than the average mass of a star on sequence B and that the mass variation across sequence A is of a similar magnitude, with the more massive stars on the shorter period side of the sequence. In general, the masses of stars at a fixed luminosity on adjacent sequences are found to increase by $\sim 16\text{--}26\%$ towards the shorter period sequence. Fitting pulsation models to the period ratios in multimode pulsators shows that the sequences C, C', B, A and A' correspond to pulsation in radial orders 1 to 5, respectively (with radial order 1 corresponding to the fundamental mode). Closely-spaced modes revealed by the period ratios in individual stars show the presence of nonradial modes. The observed period ratios indicate the presence of the $\ell = 0, 1$ and 2 modes on sequence A (radial order 4) and the $\ell = 0$ and 1 modes on sequence B (radial order 3). The relative populations and amplitudes of the modes of different ℓ show that the $\ell = 1$ mode is the most common and of the largest amplitude in both sequences. The positions of secondary mode sequences relative to primary mode sequences in the PL diagram also suggest that the $\ell = 1$ mode is the most prominent primary and secondary mode on sequences A', A and B and that the $\ell = 0$ mode is the most prominent primary and secondary mode on sequences C' and C. This result is supported by the good fit of the period ratios in radial pulsation models to the observed period ratios.

ACKNOWLEDGMENTS

I thank the anonymous referee whose constructive and detailed comments have considerably improved the readability of the paper.

REFERENCES

- Bessell M. S., Scholz M., Wood P. R., 1996, *A&A*, 307, 481
 Cardelli J. A., Clayton G. C., Mathis J. S., 1989, *ApJ*, 345, 245
 Carpenter J. M., 2001, *AJ*, 121, 2851
 Derekas A., Kiss L. L., Bedding T. R., Kjeldsen H., Lah P., Szabó G. M., 2006, *ApJ*, 650, L55
 Dziembowski W. A., Gough D. O., Houdek G., Sienkiewicz R., 2001, *MNRAS*, 328, 601
 Dziembowski W. A., Soszyński I., 2010, *A&A*, 524, AA88
 Hinkle K. H., Lebzelter T., Joyce R. R., Fekel F. C., 2002, *AJ*, 123, 1002
 Fox M. W., Wood P. R., 1982, *ApJ*, 259, 198
 Houdashelt M. L., Bell R. A., Sweigart A. V., Wing R. F., 2000, *AJ*, 119, 1424
 Houdashelt M. L., Bell R. A., Sweigart A. V., 2000, *AJ*, 119, 1448
 Ireland M. J., Scholz M., Wood P. R., 2008, *MNRAS*, 391, 1994
 Ita Y., et al., 2002, *MNRAS*, 337, L31
 Ita Y., et al., 2004, *MNRAS*, 347, 720
 Keller S. C., Wood P. R., 2006, *ApJ*, 642, 834
 Kiss L. L., Bedding T. R., 2003, *MNRAS*, 343, L79
 Mosser B., et al., 2013, *A&A*, 559, AA137
 Nicholls C. P., Wood P. R., Cioni M.-R. L., Soszyński I., 2009, *MNRAS*, 399, 2063
 Nicholls C. P., Wood P. R., Cioni M.-R. L., 2010, *MNRAS*, 405, 1770
 Nicholls C. P., Wood P. R., 2012, *MNRAS*, 421, 2616
 Nie J. D., Wood P. R., Nicholls C. P., 2012, *MNRAS*, 423, 2764
 Nie J. D., Wood P. R., 2014, *AJ*, 148, 118
 Olivier E. A., Wood P. R., 2003, *ApJ*, 584, 1035
 Skrutskie M. F., et al., 2006, *AJ*, 131, 1163
 Soszyński I., Udalski A., Kubiak M., Szymanski M., Pietrzynski G., Zebrun K., Szewczyk O., Wyrzykowski L., 2004a, *AcA*, 54, 129
 Soszyński I., et al., 2004b, *AcA*, 54, 347
 Soszyński I., et al., 2007, *AcA*, 57, 201
 Soszyński I., et al., 2009, *AcA*, 59, 239
 Soszyński I., Wood P. R., 2013, *ApJ*, 763, 103
 Soszyński I., Wood P. R., Udalski A., 2013, *ApJ*, 779, 167
 Stello D., et al., 2014, *ApJ*, 788, LL10
 Stothers R. B., 2010, *ApJ*, 725, 1170
 Tabur V., Bedding T. R., Kiss L. L., Giles T., Derekas A., Moon T. T., 2010, *MNRAS*, 409, 777
 Takayama M., Saio H., Ita Y., 2013, *MNRAS*, 431, 3189
 Takayama M., Wood P. R., Ita Y., 2015, *MNRAS*, in press
 Wood P. R., Sebo K. M., 1996, *MNRAS*, 282, 958
 Wood P. R., et al., 1999, *IAUS*, 191, 151
 Wood P. R., 2000, *PASA*, 17, 18
 Wood P. R., Olivier E. A., Kawaler S. D., 2004, *ApJ*, 604, 800
 Wood P. R., Olivier E. A., 2014, *MNRAS*, 440, 2576